

Adaptive time delay based control of non-collocated oscillatory systems

Michael Ruderman

University of Agder
P.B. 422, Kristiansand, 4604, Norway
email: michael.ruderman@uia.no

Abstract: Time delay based control, recently proposed for non-collocated fourth-order systems, has several advantages over an observer-based state-feedback cancelation of the low-damped oscillations. In this paper, we discuss a practical infeasibility of such observer-based approach and bring forward the application of the time delay based controller – simple in both the structure and design. A robust estimation of the output oscillation frequency is used and extended, in this work, by a bias cancelation that is required for tracking the oscillatory load. This way, an adaptive tuning of the time delay based controller is realized which does not require knowledge of the mass and stiffness parameters. The results are demonstrated on the oscillatory experimental setup with constraints in both the operation range and control value.

1. INTRODUCTION

Multi-mass systems with oscillatory passive loads are common in various control applications. A broad class of such cases can be approximated by fourth-order dynamics where the first active body includes the whole actuator plant, while the second passive body represents the whole payload to be controlled. Elastic links with inherently low damping make such systems challenging for stabilization of the undesired oscillations. Moreover, if only the load output state is available from the sensor measurements, such systems become non-collocated – that is the objective of our present study. For instance in cranes (see e.g. Vaughan et al. [2010]) and winch systems, the vertical oscillation dynamics can become essential, due to elasticities in ropes and cables. Longitudinal oscillations in hoisting systems (see e.g. Wang and van Horssen [2023]) are complex so that the output oscillation frequency becomes highly uncertain and valid only close to an operation point. Also the drill-string systems represent a case of oscillatory passive loads (with angular motion), see e.g. Besselink et al. [2015], while such vibration dynamics becomes even more non-trivial.

In this work, we consider a class of fourth-order non-collocated oscillation systems (Section 2), for which stabilization only a noisy sensing of the load output displacement is available. We first discuss in detail a practical infeasibility of the classical observer-based state-feedback design with reshaping of the poles location (Section 3). We show that even a low measurement noise, in combination with force and displacement constraints of the actuator, makes such a theoretically sound stabilization concept less usable. Then, it is shown (in Section 4) that the recently proposed time delay based control (Ruderman [2021, 2023]) constitutes a suitable robust alternative for such class of the systems. Also an adaptive online tuning of the oscillation frequency, required for the controller's parametrization, is shown while extending the robust estimator (Ruderman [2023]). The design of the time delay based stabilization is simple and relies on system charac-

teristics in frequency domain. Here we recall that analysis of systems with time delay(s) is well manageable with use of the corresponding transfer functions, see e.g. Kao and Lincoln [2004]. For tutorial and backgrounds on the time-delay systems we also refer to Gu et al. [2003], Michiels and Niculescu [2014], Fridman [2014]. The experimental evaluation is provided in Section 5, with the adaptive frequency tuning and also additional external disturbances.

2. NON-COLLOCATED FOURTH-ORDER SYSTEM

2.1 General framework

We consider a general framework of the non-collocated fourth-order systems, as schematically depicted in Fig. 1. The system has an active and a passive mass m and M , correspondingly. The relative motion is actuated by the constrained force $f \in [f_{\min}, f_{\max}]$ and has one degree of freedom in the shifted (against each other) coordinates (z, \dot{z}) and (y, \dot{y}) . Both inertial bodies are connected by

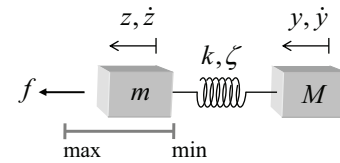


Fig. 1. General framework of non-collocated system.

an elastic link (i.e. spring), with the linear stiffness and damping coefficients k and ζ , respectively. In addition, the first active mass can be subject to the linear damping σ (equivalent to the viscous friction in an actuator), while the second passive mass can be low-damped or even undamped, – a challenging case we study also with experiments in this work. Both moving bodies can be additionally affected by the known constant (or slowly varying) loads φ and Φ , individually, or disturbances in general. Further essential assumption is that the active mass has a constrained motion range

$$z \in (z_{\min}, z_{\max}), \quad (1)$$

the fact which is often occurring due to mechanical limits of an actuator. With the above assumptions, the motion dynamics within the displacement range (1) is given by

$$m\ddot{z} + (\sigma + \zeta)\dot{z} + k(z - y) + \zeta\dot{y} + \varphi = f, \quad (2)$$

$$M\ddot{z} - \zeta(\dot{z} - \dot{y}) - k(z - y) + \Phi = 0. \quad (3)$$

The link damping $\zeta > 0$ is assumed to be relatively low, so that the load motion of an uncontrolled system in the (y, \dot{y}) coordinates experience a long-term oscillatory (and parasitic for applications) behavior. One of the most challenging (for control) characteristics of the system class (2), (3) is the non-collocation of the control value f and available output of interest y . Note that $y(t)$ is the single measurable system state, and can be also corrupted by the sensor noise. Furthermore we note that all trajectories in the four-dimensional state-space of (2), (3) are continuous and smooth within (1), while for $z = z_{\min} \vee z_{\max}$ the switchings appear (see e.g. Liberzon [2003] for basics on the switched dynamics). This is especially relevant for a constrained motion, addressed later in sections 2.2, 3.2 as a performance and feasibility limiting factor.

2.2 Experimental case study

The present experimental case study is a non-collocated fourth-order system under gravity, with a contactless output sensing, see Fig. 2. The actuated active body is the voice-coil-motor with the bounded input and output

$$u \in [0, 10] \text{ V}, \quad \text{and} \quad z \in [0, 0.021] \text{ m},$$

respectively, and an additional time constant which yields

$$f(s) = F(s)u(s) = \frac{\kappa}{\tau s + 1} u(s) = \frac{3.2811}{0.0012s + 1} u(s), \quad (4)$$

written in Laplace domain with the complex variable s . The relative displacement of the passive load is measured remotely by an inductive distance sensor, which has $\pm 12 \mu\text{m}$ nominal repeatability and a relatively large level of noise. The latter is due to the contactless measurement and dynamic misalignments of the moving body with respect to the inductive field cone of the sensor. Recall that there is no bearing for the load mass which is, this way, constituting a free-hanging body. Further details about the experimental system can be looked in Ruderman [2022, 2023]. For the vector of state variables



Fig. 2. Experimental setup of non-collocated system.

$x \equiv (x_1, x_2, x_3, x_4)^\top = (\dot{z}, z, \dot{y}, y)^\top$, the corresponding to (2), (3) state-space model is

$$\dot{x} = Ax + Bf + D, \quad (5)$$

$$y = Cx,$$

with

$$A = \begin{pmatrix} -333.35 & -333.33 & 0.015 & 333.33 \\ 1 & 0 & 0 & 0 \\ 0.012 & 266.66 & -0.012 & -266.66 \\ 0 & 0 & 1 & 0 \end{pmatrix},$$

$$B = (1.667, 0, 0, 0)^\top, \quad C = (0, 0, 0, 1), \quad \text{and}$$

$$D = (-9.806, 0, -9.806, 0)^\top.$$

Worth noting is that the disturbance vector D , cf. (2), (3), is composed by the constant gravity terms acting on both moving bodies. Further we stress that the system (5) has one conjugate-complex pole-pair with natural frequency $\omega_0 = 16.4 \text{ rad/sec}$ and extremely low damping ratio $\delta = 0.031$. The numerical parameter values of the system model were identified, partially from the available technical data-sheets of components and partially through a series of dedicated experiments, cf. e.g. Ruderman [2021], Voß et al. [2022]. An exemplary comparison between the measured and modeled output response is shown in Fig. 3 for a free fall scenario. That means starting from non-zeros initial conditions and having $f(t) = \text{const}$ for gravity compensation, the control input is then switched off at $t = 20 \text{ sec}$. This leads to $f(t) = 0$ for $t > 20$ and a fall down of both masses, while $|\dot{z}| < |\dot{y}|$ due to the actuator bearing. Hence, the oscillatory behavior becomes largely excited once $z = 0$. Note that while the the oscillation frequency

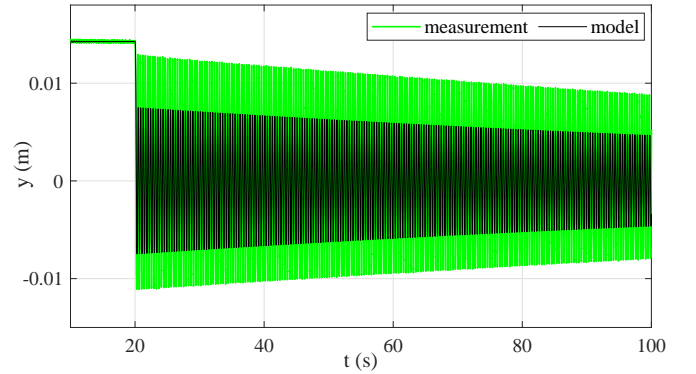


Fig. 3. Comparison of measured and computed oscillatory response of free fall scenario ($f(t) = 0$ for $t > 20 \text{ s}$).

$\omega = \omega_0 \sqrt{1 - \delta^2}$, the damping ratio, and the steady-state values are well in accord between the measurement and model, the oscillations amplitude is sensitive to both, the initial conditions and exact knowledge of the moving mass and stiffness coefficient, cf. Fig. 3.

3. OBSERVER-BASED STATE-FEEDBACK

3.1 Theoretical framework

The system dynamics (5), after compensating for the known disturbances D by feedforwarding, can be arbitrary shaped by a state feedback $-Kx$, provided the control gain

$K \in \mathbb{R}^{4 \times 1}$ is designed appropriately. That means the new system matrix $A^* = A - BK$ of the state feedback closed loop system must be Hurwitz. Furthermore, A^* should admit for the real eigenvalues only, in order to compensate for parasitic output oscillations. Note that below we will consider the state-feedback control part only, i.e. without any pre-filter, correspondingly forward gain applied to the reference value r . This is justified since our main focus in this section is put on the stability and compensation of output oscillations, and not on the reference tracking.

Since $y(t)$ is the only available system measurement, a natural way to keep usage of the state-feedback control is to design an asymptotic state observer Luenberger [1971], also well known as Luenberger observer. The system (5) proves to be fully observable so that an observation gain $Q \in \mathbb{R}^{4 \times 1}$ can be determined so that to provide estimate \tilde{x} of the state vector. The corresponding block diagram of

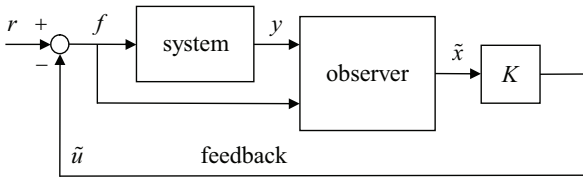


Fig. 4. Block diagram of the state-feedback with observer.

a state-feedback control with observer is shown in Fig. 4. Recall that for an asymptotically stable observation error $e(t) = x(t) - \tilde{x}(t)$, i.e. for

$$\lim_{t \rightarrow \infty} \|e(t)\| = 0,$$

the system matrix of the observation error dynamics

$$\dot{e}(t) = \tilde{A}e(t) = (A - QC)e(t),$$

must be Hurwitz. For ensuring the asymptotic observer operates efficiently in combination with a state-feedback control, the corresponding poles of \tilde{A} are required to be significantly faster than those of A^* . Also recall that once the state-feedback which is including observer is closed, cf. Fig. 4, the state estimation dynamics becomes

$$\dot{\tilde{x}} = (A - BK - QC)\tilde{x} + Bf + Qy. \quad (6)$$

Despite the well-known separation principle of designing Luenberger observer, that allows the poles of observer and state-feedback to be assigned stable and independent of each other, a practical realization of the closed loop as in Fig. 4 reveals infeasible for the system class introduced in section 2.1. Next, we are to show it, while stressing that an observer-based state-feedback control as in Fig. 4 is well established and acknowledged (also in applications) for multiple types of the systems with observable dynamics.

3.2 Practical infeasibility

While the designed observer and the state-feedback loop based on it both have a stable pole dynamics, we are to address additional stability features, that from a loop transfer function point of view, cf. Fig. 4. The observer-based open loop transfer function from $r(s)$ to $\tilde{u}(s)$ is

$$L_o(s) = K(sI - A + BK + QC)^{-1} [BQ] \begin{bmatrix} 1 \\ G(s) \end{bmatrix} \quad (7)$$

with

$$G(s) = C(sI - A)^{-1}B.$$

Recall that without use of observer (i.e. if the full state $x(t)$ is measurable), the open loop transfer function is given by

$$L_m(s) = K(sI - A)^{-1}B. \quad (8)$$

Note that in both above cases, the open loop transfer functions are not including the additional (disturbing) actuator dynamics $F(s)$, cf. (4). Therefore, also the corresponding open loop transfer functions $F(s)L_o(s)$ and $F(s)L_m(s)$, respectively, will be inspected for analyzing the practical infeasibility. Now, let us make use of the so-called stability margin or *maximum sensitivity* (see e.g. Åström and Murray [2021] for details), which is defined as maximum magnitude, i.e.

$$S_{\max} = \max_{\Omega} |S(i\Omega)| = \max_{\Omega} |(1 + L(i\Omega))^{-1}|, \quad (9)$$

of the corresponding sensitivity function $S(\cdot)$ of any open loop transfer function $L(\cdot)$. The latter is evaluated in frequency domain, where Ω in the angular frequency variable and i is the imaginary unit satisfying $i^2 = -1$. Recall that S_{\max} indicates how close the Nyquist plot of the open loop transfer function bypasses from the right the critical point $(-1, 0)$ in the complex plane, cf. Åström and Murray [2021]. Thus, it represents a stability's capacity feature of the closed loop system and is, typically, required to be $S_{\max} < 2 = 6$ dB. Systems to have the loop transfer function with $S_{\max} > 4 = 12$ dB indicate poor performance as well as poor robustness, cf. Skogestad and Postlethwaite [2005]. Further we note that for the closed loop system structure as in Fig. 4, the sensitivity function represents transfer characteristics between the reference value and input to the system plant.

Consider a pole placement design of the above stated observer and the enclosing state-feedback control loop for the system (5). The assigned real poles of the state feedback control are $\lambda_c = \{-40, -42, -44, -60\}$ and those of the asymptotic observer are $\lambda_o = \{-498, -503, -508, -513\}$. Note that the poles are placed sufficiently close to each other, thus providing an approximately same time-scale of the corresponding eigenbehaviors. Moreover, the observer's poles are approximately two and a half times faster than those of the closed loop. All four sensitivity functions, with and without the use of observer and both also incorporating the actuator dynamics, are shown in Fig. 5. One can recognize that already the state-feedback without observer has a relatively poor stability margin. When using observer, the S_{\max} peak is further growing and becomes sharper, and in case of an additional actuator dynamics reaches 13.4 dB value. Worth recalling is that a step reference will excite all frequencies so that the input constraints (cf. section 2.1) becomes violated at transients.

The implemented model (1)–(5) is used in numerical simulation of the state-feedback control with and without observer designed as above. The simulated output $y(t)$ is subject to a minor (lower than in the experimental system) measurement noise. Also the step reference $r(t)$ is chosen so that the state-feedback control without observer is not saturated, cf. section 2.2. The fixed-step solver with the sampling time 0.0002 sec (same as in the real-time experiments) is used. The output response and control value out from simulation are shown for both cases in Fig.

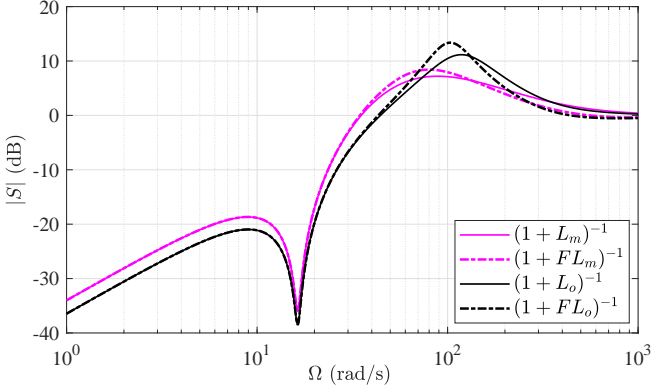


Fig. 5. Sensitivity function of state-feedback control loop with and without the use of observer.

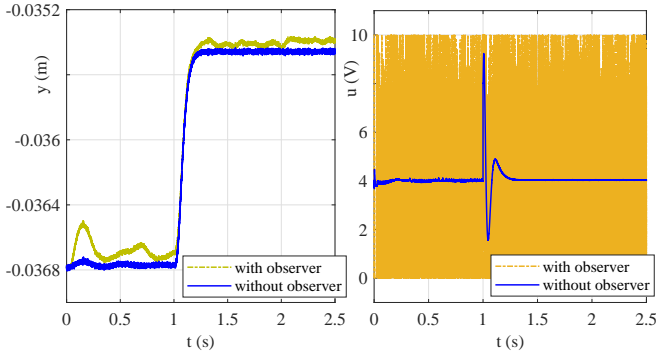


Fig. 6. Simulated response with and without observer.

6. One can see that in case of observer, the control value comes permanently in a high-frequency saturated behavior, that makes the control practically infeasible.

4. TIME DELAY BASED CONTROL

4.1 Time delay based control

The time delay based feedback control of fourth-order oscillatory systems, initially proposed in Ruderman [2021], is analyzed in detail in Ruderman [2023], also with experimental evaluation in combination with a standard PI-controller. The time delay based control

$$u_d(t) = \alpha(y(t) - y(t - \theta)), \quad (10)$$

relies on the knowledge of the system parameter ω , and assumes the time delay constant

$$\theta = -\arg[G(i\omega)]\omega^{-1}, \quad (11)$$

and the gaining factor $\alpha > 0$ which is design parameter. The system transfer function in frequency domain is

$$G(i\Omega) = \frac{y(i\Omega)}{u(i\Omega)} = C(i\Omega I - A)^{-1}B, \quad (12)$$

and I is the identity matrix of the appropriate dimension.

Recall that the time delay based control (10) is largely attenuating the system resonance peak (around ω_0) without much reshaping the $G(i\Omega)$ transfer characteristics at other frequencies. Expressing the transfer function (12) as a ratio $G(i\Omega) = N(i\Omega)P(i\Omega)^{-1}$ of the corresponding polynomials $N(\cdot)$ and $P(\cdot)$, and rewriting (10) in frequency domain as

$$U_d(i\Omega) = \alpha(1 - \exp(-i\Omega\theta)), \quad (13)$$

one can show that the closed loop $G_{cl} = N(P - NU_d)^{-1}$ is reshaping the system transfer characteristics as

$$R(i\Omega) = \frac{G(i\Omega)}{G_{cl}(i\Omega)} = 1 - \frac{N(i\Omega)U_d(i\Omega)}{P(i\Omega)}. \quad (14)$$

The reshaping (14) of the transfer characteristics of the system (5), here without constant disturbance D and setting in (4) $\tau = 0$, is exemplary shown in Fig. 7 for $\alpha = 100$. One can recognize that the principal difference between

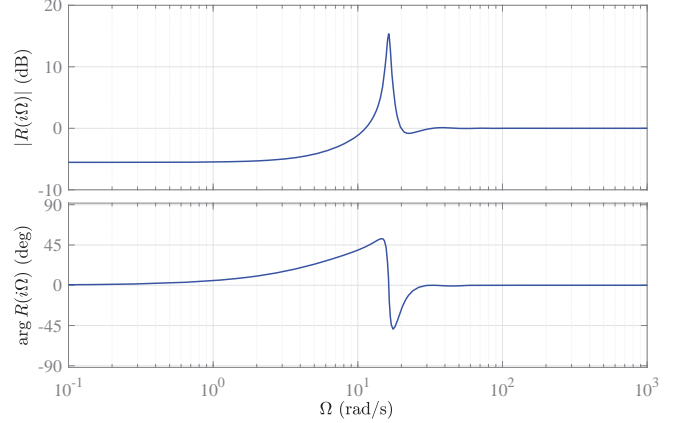


Fig. 7. Reshaping (14) of system transfer characteristics.

the original system $G(i\Omega)$ and that one with the time delay based compensator, i.e. $G_{cl}(i\Omega)$, is the resonance peak of $G(i\Omega)$. At higher frequencies, there is no changes in the amplitude response, while at lower frequencies an acceptable gain reduction is by approximately -5 dB. This can be reasonably taken into account when the resonance-compensated system $G_{cl}(i\Omega)$ will be closed by an outer tracking control, cf. Ruderman [2023]. One can also recognize that the phase response of $G(i\Omega)$ and $G_{cl}(i\Omega)$ are essentially the same to left- and right-hand-side of the resonance frequency.

4.2 Robust frequency estimator

The robust frequency estimator, proposed in Ruderman [2022], can be used for online tuning of the ω -parameter, provided the measured oscillatory signal $w(t)$ in unbiased. The estimator dynamics is given by, cf. Ruderman [2022],

$$\begin{pmatrix} \dot{\eta}_1 \\ \dot{\eta}_2 \end{pmatrix} = \begin{pmatrix} 0 & 1 \\ -\tilde{\omega}^2 & -2\tilde{\omega} \end{pmatrix} \begin{pmatrix} \eta_1 \\ \eta_2 \end{pmatrix} + \begin{pmatrix} 0 \\ 2\tilde{\omega} \end{pmatrix} w, \quad (15)$$

$$\nu = \begin{pmatrix} 0 & 1 \end{pmatrix} \begin{pmatrix} \eta_1 \\ \eta_2 \end{pmatrix},$$

with the adaptation law

$$\dot{\tilde{\omega}} = -\gamma \tilde{\omega} \text{sign}(\eta_1)(w - \nu), \quad (16)$$

which has $\gamma > 0$ as the parameter gain to be assigned. Note that the right-hand-side of (16) includes (additionally in comparison to Ruderman [2022]) a multiplication by $\tilde{\omega}$, so as to avoid the frequency estimate $\tilde{\omega}$ bypassing into the negative range. For details on the stability and performance of the robust frequency estimator the reader is referred to Ruderman [2022].

In order for a biased oscillation output $y(t)$ can equally be used in the frequency estimator (15), (16), the following dynamic bias-cancellation is proposed

$$w(t) = y(t) - y\left(t - \frac{\pi}{\beta}\right), \quad \omega < \beta < 3\omega, \quad (17)$$

where β is a free adjustable time-delay parameter. Assuming a biased harmonic oscillation

$$y(t) = Y_0 + Y \sin(\omega t + \phi) \quad (18)$$

and substituting it into (17) results in

$$w(t) = Y \left(\sin(\omega t + \phi) - \sin\left(\omega t + \phi - \omega \frac{\pi}{\beta}\right) \right). \quad (19)$$

One can recognize that (19) constitutes also a harmonic signal with the same fundamental frequency ω . The signal is unbiased and has another amplitude and phase comparing to the harmonic part of (18). Also worth noting is that $w(t)$ is not zero signal as long as $\omega\pi\beta^{-1} \neq 0$. If some nominal (or upper bound) value of ω is known, the phase shifting factor β can be assigned in a relatively large range, cf. (17). Since the robust estimator (15), (16) is insensitive

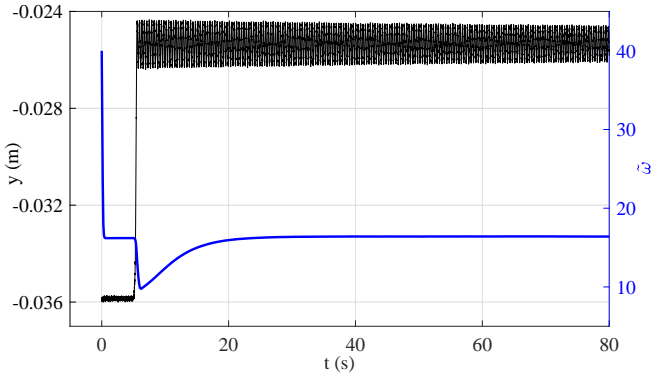


Fig. 8. Converging $\tilde{w}(t)$ versus measured oscillating $y(t)$.

to both, the phase ϕ and slow variations of Y , see Ruderman [2022], the bias-free input (19) can directly be used for estimation of \tilde{w} . Recall that $\tilde{w}(t)$ has a convergence behavior which rate is controllable by γ . An exemplary convergence of \tilde{w} is shown together with the used $y(t)$ measurement in Fig. 8. Note that the measured output is biased before and after the step-wise excitation. The initial value is set to $\tilde{w}(0) = 40$ and the gain to $\gamma = 200$. One can recognize that after the exciting transient of $y(t)$, the $\tilde{w}(t)$ is re-converging towards its final value ≈ 16.4 rad/sec.

5. EXPERIMENTAL CONTROL EVALUATION

The standard PI feedback controller

$$u_{pi}(t) = K_p e(t) + K_i \int e(t) dt, \quad (20)$$

operating on the output error $e(t) = r(t) - y(t)$ with $r(t)$ to be the set reference value for oscillatory load, can be desirable for the following reasons. (i) The single available system state is $y(t)$. (ii) An integral control action is required for guaranteeing a steady-state accuracy. (iii) An additional differential control action (i.e. resulting in PID control) is not contributing to stabilization of the oscillatory load in the fourth-order system (5). (iv) a state-feedback control, that requires an additional state observer, fails practically for the systems (2), (3), as discussed in section 3. At the same time, one can show that the open loop transfer function $L(i\Omega) = y(s)/r(s) = PI(i\Omega)G(i\Omega)$, where $PI(i\Omega)$ is the transfer function corresponding to

(20) has a marginal (or even none) gain margin. For basics on the gain margin and loop transfer function analysis we refer to e.g. Franklin et al. [2020]. Also the so-called maximum sensitivity (cf. e.g. Åström and Murray [2021]) has a relatively high number for the corresponding $S(i\Omega) = (1 + L(i\Omega))^{-1}$, cf. section 3, that indicates low capacity of stability for the closed loop system.

The overall control law, experimentally evaluated, is

$$u(t) = u_{pi}(t) + u_d(t) + 4.035, \quad (21)$$

where the last constant right-hand-side term compensates for the known gravity disturbance, cf. (2), (3), (4). Note that for the assigned $K_p = 100$, $K_i = 170$, cf. Ruderman [2023], the loop transfer function $L(\cdot)$ (i.e. without (13)) has a sufficient phase margin of 46 deg, but the missing gain margin of -4.2 dB.

First, the closed loop response controlled with (21) is experimentally evaluated, shown in Fig. 9, once without the time delay control part (i.e. with $\alpha = 0$) and once with the time delay control part with $\alpha = 100$. Note that here a fixed time delay constant, cf. section 4.1, is assigned from the known system parameter ω . While the time delay

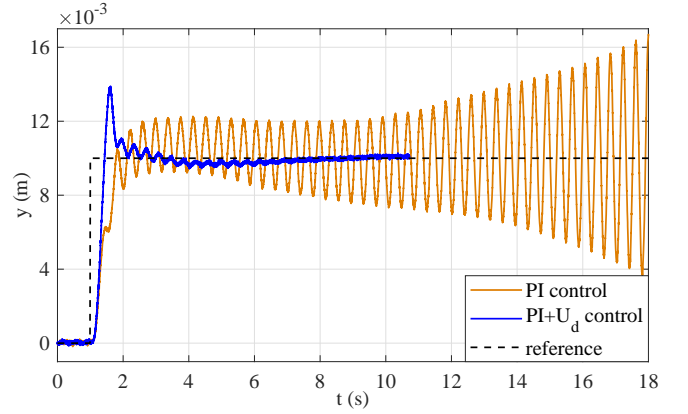


Fig. 9. Controlled $y(t)$ by PI control (i.e. $\alpha = 0$) and $PI + U_d$ control with $\alpha = 100$ and fixed θ value.

based control provides a relatively fast cancelation of the otherwise oscillating output, cf. Fig. 3, the pure PI control drives the system to a visible instability over the time.

Next, the feedback control (21) is experimentally evaluated when applying an online adaptation of θ by means of the robust frequency estimator described in section 4.2. The adaptation gain is assigned to $\gamma = 600$. The results are shown in Fig. 10, where the controlled output is depicted in (a), and the time progress of the $\tilde{w}(t)$ estimate is depicted in (b). Also the manual mechanical disturbances, which are additionally exciting the output oscillations, were applied, once by pushing down and once by pushing up the passive load, see in Fig. 10 (a) marked by the arrows. One can recognize both, a stable attenuation of the output oscillations and robust convergence of the $\tilde{w}(t)$ estimate. Important to notice is that due to some (none modeled) nonlinear by-effects in stiffness, the oscillation frequency ω experiences certain variations depending on the amplitude of $y(t)$, here elongation of the spring.

As further evaluation of robustness of the adaptive control (21) that includes online estimation of \tilde{w} , the experiments

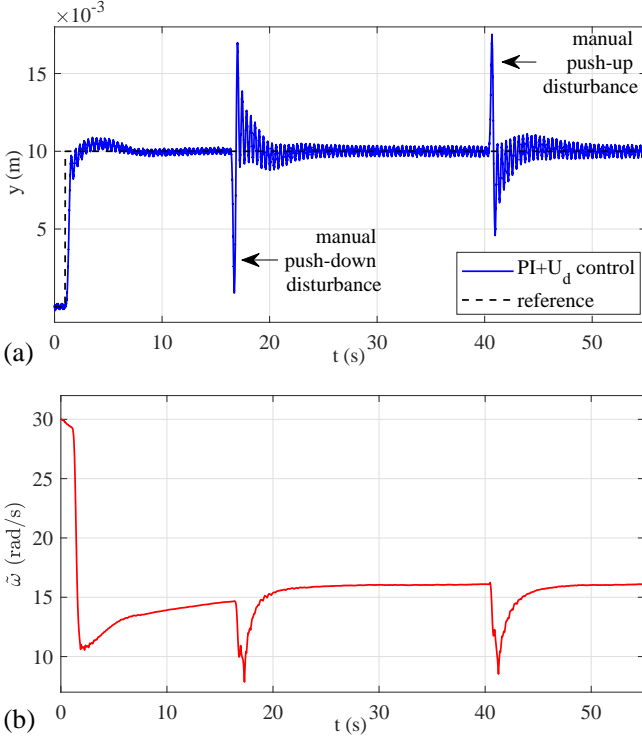


Fig. 10. Controlled $y(t)$ with $PI + U_d$ and $\alpha = 100$ and online adapted θ in (a), disturbance instants are marked; and convergence of $\tilde{\omega}(t)$ in (b).

with the same control parameters as above are performed for oscillatory initial conditions, see Fig. 11. One can recognize a largely oscillating $y(t)$ value before the step reference is applied. For largely (i.e. more pronounced)

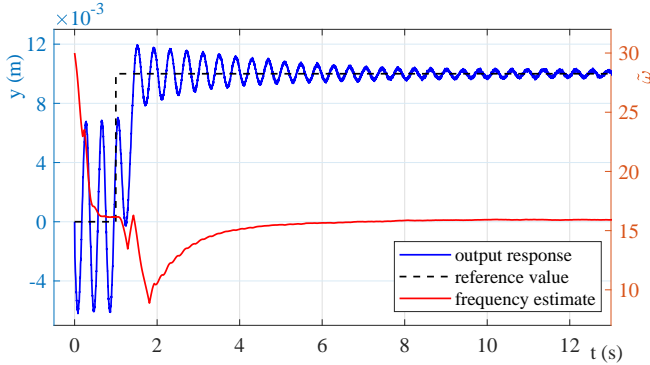


Fig. 11. Controlled $y(t)$ by the $PI + U_d$ control with $\alpha = 100$ and oscillatory initial conditions versus the convergence of $\tilde{\omega}(t)$.

oscillations of $y(t)$, the $\tilde{\omega}(t)$ experiences a fast convergence, which is then perturbed by the output transient for which $Y_0 \neq \text{const}$, cf. (18). After the transient, the convergence of $\tilde{\omega}(t)$ recovers again.

6. CONCLUSIONS

In this paper, we have discussed the fourth-order non-collocated systems with low damped oscillating passive loads. Approaching the applications, an actuator body is subject to the input and output constraints. We an-

alyzed and demonstrated numerically that an observer-based state-feedback control reveals infeasible, despite the system dynamics proves to be observable. As a robust alternative, the time delay based control (Ruderman [2021, 2023]) was applied for stabilizing the otherwise unstable PI set reference controller. The bias-canceling extension of the robust frequency estimator (Ruderman [2022]) was introduced that allows for an online (adaptive) tuning of the time delay based controller. Various dedicated experiments were shown as confirmatory.

REFERENCES

- Åström, K.J. and Murray, R.M. (2021). *Feedback systems: an introduction for scientists and engineers*. Princeton University Press.
- Besselink, B., Vromen, T., Kremers, N., and Van De Wouw, N. (2015). Analysis and control of stick-slip oscillations in drilling systems. *IEEE Trans. on Cont. Syst. Techn.*, 24(5), 1582–1593.
- Franklin, G., Powell, J., and Emami-Naeini, A. (2020). *Feedback control of dynamic systems*. Pearson.
- Fridman, E. (2014). Tutorial on lyapunov-based methods for time-delay systems. *European Journal of Control*, 20(6), 271–283.
- Gu, K., Kharitonov, V., and Chen, J. (2003). *Stability of time-delay systems*. Springer.
- Kao, C.Y. and Lincoln, B. (2004). Simple stability criteria for systems with time-varying delays. *Automatica*, 40(8), 1429–1434.
- Liberzon, D. (2003). *Switching in systems and control*. Springer.
- Luenberger, D. (1971). An introduction to observers. *IEEE Trans. on Automatic Control*, 16(6), 596–602.
- Michiels, W. and Niculescu, S.I. (2014). *Stability, control, and computation for time-delay systems: an eigenvalue-based approach*. SIAM.
- Ruderman, M. (2021). Robust output feedback control of non-collocated low-damped oscillating load. In *IEEE 29th Mediterranean Conference on Control and Automation (MED)*, 639–644.
- Ruderman, M. (2022). One-parameter robust global frequency estimator for slowly varying amplitude and noisy oscillations. *Mechanical Systems and Signal Processing*, 170, 108756.
- Ruderman, M. (2023). Time-delay based output feedback control of fourth-order oscillatory systems. *Mechatronics*, 94, 103015.
- Skogestad, S. and Postlethwaite, I. (2005). *Multivariable feedback control: analysis and design*. John Wiley & Sons.
- Vaughan, J., Kim, D., and Singhose, W. (2010). Control of tower cranes with double-pendulum payload dynamics. *IEEE Trans. on Cont. Syst. Techn.*, 18(6), 1345–1358.
- Voß, B., Ruderman, M., Weise, C., and Reger, J. (2022). Comparison of fractional-order and integer-order H-infinity control of a non-collocated two-mass oscillator. *IFAC-PapersOnLine*, 55, 145–150.
- Wang, J. and van Horssen, W.T. (2023). On resonances and transverse and longitudinal oscillations in a hoisting system due to boundary excitations. *Nonlinear Dynamics*, 111, 5079–5106.